Direct Torque Control With Feedback Linearization for Induction Motor Drives

Cristian Lascu, Saeed Jafarzadeh, *Member, IEEE*, M. Sami Fadali, *Senior Member, IEEE*, and Frede Blaabjerg, *Fellow, IEEE*

***Abstract*—This paper describes a direct-torque-controlled (DTC) induction motor (IM) drive that employs feedback linearization and sliding-mode control (SMC). A new feedback linearization approach is proposed, which yields a decoupled linear IM model with two state variables: torque and stator flux magnitude. This intuitive linear model is used to implement a DTC-type controller that preserves all DTC advantages and eliminates its main drawback, the flux and torque ripple. Robust, fast, and ripple-free control is achieved by using SMC with proportional control in the vicinity of the sliding surface. SMC assures robustness as in DTC, while the proportional component eliminates the torque and flux ripple. The torque time response is similar to conventional DTC and the proposed solution is flexible and highly tunable due to the *P* component. The controller design is presented, and its robust stability is analyzed in simulations. The sliding controller is compared with a linear DTC scheme with and without feedback linearization. Extensive experimental results for a sensorless IM drive validate the proposed solution.**

***Index Terms*—Adjustable speed drives, direct torque control (DTC), feedback linearization, induction motor (IM) drives, sliding-mode control (SMC).**

I. Introduction

DIRECT torque control (DTC) is a robust, fast-responding control strategy for induction machine (IM) drives [1], [2]. Conventional DTC employs closed-loop hysteresis torque and flux controllers and a switching table to select the voltage vector applied to the motor. DTC achieves rapid and robust torque and flux control without using current controllers. DTC operation is associated with large torque ripple, which causes noise, vibrations, and increased losses, while the switching frequency of the voltage source inverter (VSI) is variable and low. Improved DTC solutions that run at constant switching frequency and use modern control theory have recently been developed to reduce the torque ripple. Novel DTC strategies based on discrete space vector modulation (SVM) techniques are described in [3]. DTC based on linear torque and flux controllers (linear DTC) and SVM was introduced in [4]. Several schemes using the variable structure control principles have been proposed in [5].

Feedback linearization (FBL) is a nonlinear control approach. The main idea of FBL is to transform a nonlinear system into an equivalent linear system, design a linear controller for the linear system, and then use the inverse transformation to obtain the desired controller for the original nonlinear system. Because the method is sensitive to modeling errors and disturbances, it has been rarely applied to IM drives. FBL is used in [6]–[12] to linearize the IM model with respect to speed, flux, and current. Two linearization schemes in which only one control quantity is transformed are discussed in [12]. All solutions in [6]–[12] are based on current linearization and control. Applications of FBL to power electronics and PMSM drives are presented in [13]–[20]. An error sensitivity analysis in [8] shows that the control performance may deteriorate due to perturbations, parameter detuning, and measurement errors.

Sliding-mode control (SMC) is a robust control technique well suited for control systems with uncertainties or modeling errors [21]. It has been successfully applied to IM drives and provides excellent dynamic performance for a wide speed range operation [5], [7], [19]–[24]. The switching behavior can be integrated with the VSI operation as shown in [21]. In fact, the conventional DTC is a form of SMC, which was designed to closely match the switching nature of the VSI.

This paper proposes a new DTC controller that integrates feedback linearization together with SMC. The main advantage of FBL over classical DTC is that the linear control theory results can easily be applied to obtain a better performance. We use this property to design and then theoretically investigate the robustness and stability of the proposed control method. Moreover, the controller–observer separation principle allows the controller and the observer to be independently designed, if the plant model is approximately linear and estimation errors are small [25]. The FBL disadvantage is the sensitivity of the linearized model to uncertainties and parameter detuning, which motivates the use of SMC.

The nonlinear IM model considered in this paper is fourth order with the state variables: torque, stator flux, rotor flux, and another flux-dependent state. The feedback-linearized IM model is second order, with only the torque and stator flux magnitude as decoupled state variables. Thus, the new linear model is intuitive, very simple, and it substantially simplifies the controller design. The flux and torque are controlled by the new DTC scheme and the proposed controllers employ SMC to maintain robust sensorless operation of the drive. This approach based on

Manuscript received January 20, 2016; revised March 24, 2016; accepted April 24, 2016. Date of publication May 9, 2016; date of current version December 9, 2016. Recommended for publication Associate Editor by B. Wang.

C. Lascu is with the Department of Electrical Engineering, University Politehnica of Timisoara, Timisoara 300223, Romania (e-mail: cristian.lascu@et.upt.ro).

S. Jafarzadeh is the Department of Computer and Electrical Engineering and Computer Science, California State University Bakersfield, Bakersfield, CA 93311 USA (e-mail: sjafarzadeh@csub.edu).

M. Sami Fadali is the Department of Electrical and Biomedical Engineering, University of Nevada Reno, Reno, NV 89557 USA (e-mail: fadali@unr.edu).

F. Blaabjerg is with the Department of Energy Technology, Aalborg University, Aalborg East 9220, Denmark (e-mail: fbl@et.aau.dk).

Color versions of one or more of the figures in this paper are available online at http://ieeexplore.ieee.org.

Digital Object Identifier 10.1109/TPEL.2016.2564943

torque–flux linearization and control is different from existing methods in [6]–[12], which are based on current control. The combination of these techniques preserves the fast and robust response of conventional DTC while entirely eliminating the torque and flux ripple.

II. Feedback Linearization of IM Model

Conventional linearization of a nonlinear system is based on a first-order approximation of the system dynamics at a chosen operating point while neglecting high-order dynamics. This linearization is satisfactory in many applications where normal system operation remains in the vicinity of a fixed or slowly varying equilibrium, but it is otherwise inappropriate. In particular, linearization is only appropriate for IM drives operating at constant rotor speed. Otherwise, the IM behavior is inherently nonlinear and other approaches must be used.

Feedback linearization is a technique that allows the designer to use linear control methodologies with inherently nonlinear systems such as the IM. The FBL algebraically transforms a nonlinear system model into a linear one, so that linear control techniques can be used. Unlike conventional linearization, the linearization and the linear behavior are valid globally, rather than in the vicinity of an equilibrium point [11]. In general, the linearizing transformation is quite difficult to find, but in some cases it is easy to obtain by a simple redefinition of variables [26]. Fortunately, the FBL of an IM is achievable by an intuitive transformation of the state variables and an input redefinition.

The IM state space model in the stator reference frame is

$$\frac{d\underline{\psi}_s}{dt} = -\frac{1}{T_s\sigma}\underline{\psi}_s + \frac{L_m}{L_rT_s\sigma}\underline{\psi}_r + \underline{u}_s \tag{1}$$

$$\frac{d\underline{\psi}_r}{dt} = \frac{L_m}{L_sT_r\sigma}\underline{\psi}_s - \left(\frac{1}{T_r\sigma} - j\omega_r\right)\underline{\psi}_r \tag{2}$$

where Ψ_s, Ψ_r are the stator and rotor flux space vectors, respectively, R_s and R_r are the stator and rotor resistances, L_s, L_r, and L_m are the stator, rotor, and magnetizing inductances, $T_s = L_s/R_s,\ T_r = L_r/R_r,\ \sigma = (L_sL_r - {L_m}^2)/L_sL_r$, ω_r is the rotor speed, and $\underline{u}_s = u_{sd} + ju_{sq}$ is the stator voltage vector, which acts as input.

The model can be linearized by selecting the new states

$$M = \psi_{sq}\psi_{rd} - \psi_{sd}\psi_{rq} \tag{3}$$

$$R = \psi_{sd}\psi_{rd} + \psi_{sq}\psi_{rq} \tag{4}$$

$$F_s = \psi_{sd}^2 + \psi_{sq}^2 \tag{5}$$

$$F_r = \psi_{rd}^2 + \psi_{rq}^2 \tag{6}$$

where M is the scaled torque and F_s and F_r are the squared magnitudes of the stator and rotor flux, respectively. The variable R depends on the rotor and stator flux. For simplicity, we refer *M* as the torque and F_s as the flux magnitude. We are primarily interested in controlling the torque M and the stator flux magnitude F_s. However, we must also insure that the remaining state variables F_r and *R* are bounded.

The IM state equations with the state variables (3)–(6) are

$$\frac{dM}{dt} = -\left(\frac{1}{T_r\sigma} + \frac{1}{T_s\sigma}\right)M - \omega_r R - \psi_{rq}u_{sd} + \psi_{rd}u_{sq} \tag{7}$$

$$\frac{dF_s}{dt} = -\frac{2}{T_s\sigma}F_s + \frac{2L_m}{L_rT_s\sigma}R + 2\psi_{sd}u_{sd} + 2\psi_{sq}u_{sq} \tag{8}$$

$$\frac{dF_r}{dt} = -\frac{2}{T_r\sigma}F_r + \frac{2L_m}{L_sT_r\sigma}R \tag{9}$$

$$\frac{dR}{dt} = -\left(\frac{1}{T_r\sigma} + \frac{1}{T_s\sigma}\right)R + \omega_r M + \frac{L_m}{L_sT_r\sigma}F_s + \frac{L_m}{L_rT_s\sigma}F_r + \psi_{rd}u_{sd} + \psi_{rq}u_{sq}. \tag{10}$$

The first three state equations are feedback linearized if the inputs are redefined as

$$w_q = -\omega_r R - \psi_{rq}u_{sd} + \psi_{rd}u_{sq} \tag{11}$$

$$w_d = \frac{2L_m}{L_rT_s\sigma}R + 2\left(\psi_{sd}u_{sd} + \psi_{sq}u_{sq}\right). \tag{12}$$

Now the linearized system is

$$\frac{dM}{dt} = -\left(\frac{1}{T_r\sigma} + \frac{1}{T_s\sigma}\right)M + w_q \tag{13}$$

$$\frac{dF_s}{dt} = -\frac{2}{T_s\sigma}F_s + w_d \tag{14}$$

$$\frac{dF_r}{dt} = -\frac{2}{T_r\sigma}F_r + \frac{2L_m}{L_sT_r\sigma}R \tag{15}$$

$$\frac{dR}{dt} = -\left(\frac{1}{T_r\sigma} + \frac{1}{T_s\sigma}\right)R + \frac{L_m}{L_sT_r\sigma}F_s + \frac{F_r}{2R}w_d - \frac{M}{R}w_q. \tag{16}$$

Solving (11) and (12) gives the control signals

$$u_{sd} = \frac{\psi_{rd}}{2R}\left(w_d - \frac{2L_m}{L_rT_s\sigma}R\right) - \frac{\psi_{sq}}{R}\left(w_q + \omega_r R\right) \tag{17}$$

$$u_{sq} = \frac{\psi_{rq}}{2R}\left(w_d - \frac{2L_m}{L_rT_s\sigma}R\right) + \frac{\psi_{sd}}{R}\left(w_q + \omega_r R\right). \tag{18}$$

FBL decouples the state variables of interest, namely, the torque M and the stator flux magnitude F_s and thus significantly simplifies the controller design for the IM drive system. In addition, since the resulting system is linear, the classical linear control methodologies can be used. Since the M, F_s, and F_r have dynamics with left plane poles, the input–output stability of the remaining state variables can be easily guaranteed provided that R stays bounded. The *R* state equation (16) shows that its right-hand side is unbounded for zero R, which only occurs in the trivial condition when the stator or rotor flux is zero. Except for the startup, this condition never occurs during regular operation. In the physical drive, the controller ensures that the flux has been installed prior to starting the drive. Simulation results in Section IV show that the torque control is started with a 40 ms delay after the flux control, when fluxes are at nominal levels. It is therefore assumed that the variable R has a lower

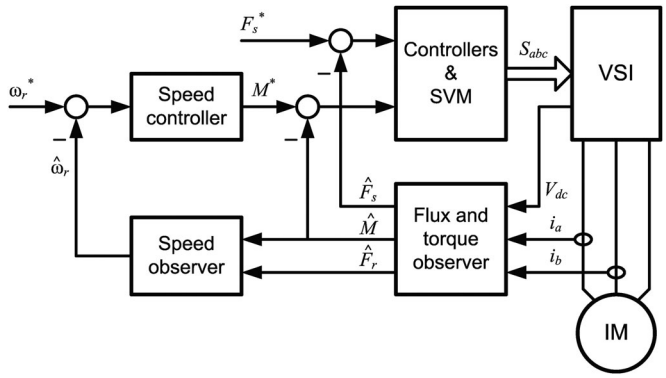

Fig. 1. Block diagram of the sensorless DTC IM drive with feedback linearization.

bound R_l. R is also upper bounded in practice because the flux magnitudes are limited due to magnetic saturation.

III. DTC via Sliding Mode

SMC is used to achieve a fast and robust operation of an IM drive. Fig. 1 shows the block diagram of the proposed drive. The block *controllers and SVM* contains the FBL and the torque and flux controllers described next. The drive uses simple speed, torque, and flux observers and a PI speed controller. Drive data and a brief description of the observers are provided in the Appendix.

The control objective is to control the torque and stator flux magnitude in the machine, i.e., to realize a DTC-type controller. To this end, we design controllers for the torque *M* and the stator flux F_s in the linearized model. Since the state (13) and (14) governing *M* and F_s, respectively, are decoupled, the design of their controllers to obtain the inputs w_d and w_q is quite simple. These are then substituted in (17) and (18) to obtain the physical inputs u_{sd} and u_{sq}, respectively. However, errors in the calculation of the physical inputs are inevitable and must be accounted for and corrected to provide robust performance.

The errors in the physical control inputs can be represented as equivalent errors in the linear state (13) and (14). Equation (13) can be rewritten in the form

$$\frac{dM}{dt} = g_M + w_q \tag{19}$$

where g_M represents the uncertain dynamics of the FBL torque equation. The term g_M is not exactly known; from (13), an estimate of the dynamics is given by

$$\hat{g}_M = -\left(\frac{1}{T_r\sigma} + \frac{1}{T_s\sigma}\right) M.$$

We assume that the estimation error for g_M is bounded as

$$|\hat{g}_M - g_M| \leq G_M. \tag{20}$$

To design the SMC for the linear system of (19), we define the sliding surface as the torque error

$$S_M = M - M_d. \tag{21}$$

For this choice of sliding surface, we use the SMC

$$w_q = -\hat{g}_M - k_M \operatorname{sgn}(S_M), \qquad k_M > 0. \tag{22}$$

The term $-k_M \operatorname{sgn}(S_M)$ is known as the corrective control.

We choose the quadratic Lyapunov function candidate $V = S_M^2/2$. The system converges to the sliding surface if the derivative of a Lyapunov function is negative along all the trajectories of the system. The derivative of *V* is

$$\begin{aligned}\frac{1}{2}\frac{d}{dt}S_M^2 &= (g_M - \hat{g}_M - k_M \operatorname{sgn}(S_M))\, S_M \\ &= (g_M - \hat{g}_M)\, S_M - k_M |S_M|. \end{aligned} \tag{23}$$

For robust convergence to the sliding surface the derivative must remain negative in the presence of uncertainties. We choose the corrective control gain k_M as in (24)

$$k_M = G_M + \eta_M. \tag{24}$$

This gives the sliding condition

$$\frac{1}{2}\frac{d}{dt}{S_M}^2 \leq -\eta_M |S_M| \tag{25}$$

where η_M is a positive constant. The gain k_M of (24) includes the term G_M to ensure robust stability and the term η_M to control the speed of convergence to the sliding controller. A bigger η_M makes the system trajectory to reach the sliding surface in a shorter time but can result in higher chattering. Similar results can be obtained by using an integral sliding surface

$$S_M = \left(\frac{d}{dt} + \lambda_M\right) \int_0^t (M - M_d)\, d\tau \tag{26}$$

where λ_M is a positive constant design parameter. This parameter determines how fast the error goes to zero once the state is on the surface. The SMC effort can be chosen as

$$w_q = -\hat{g}_M - \lambda_M (M - M_d) - k_M \operatorname{sgn}(S_M), \qquad k_M > 0 \tag{27}$$

and the sliding condition holds for $k_M = G_M + \eta_M$.

To avoid chattering, we define a boundary layer around the sliding surface $B_M(t) = \{x, |S_M(x)| \leq h_M\}$, where $h_M > 0$ is the boundary layer thickness. Inside the boundary layer, a proportional control term is added to the control of (22). Outside the boundary layer ($|S_M(x)| > h_M$), the corrective control drives the system to the sliding surface.

The stator flux dynamics in (14) are almost identical to (13) and are similarly handled. Most of the analysis is omitted, for brevity. Similarly to torque, the sliding surface is

$$S_{F_s} = F_s - F_{sd} \tag{28}$$

and the linear system control input is

$$w_d = -\hat{g}_{F_s} - k_{F_s} \operatorname{sgn}(S_{F_s}), \qquad k_{F_s} > 0. \tag{29}$$

As for torque, we use a narrow boundary layer around the sliding surface, with proportional control to avoid chattering.

Fig. 2 shows the block diagram of the SMC with FBL torque and flux controller. To summarize, the controllers are given by (22) and (29) and the reference voltages are produced by (17) and (18) in the stator reference frame. A SVM unit produces the VSI switching signals $S_a, S_b, \text{and } S_c$.

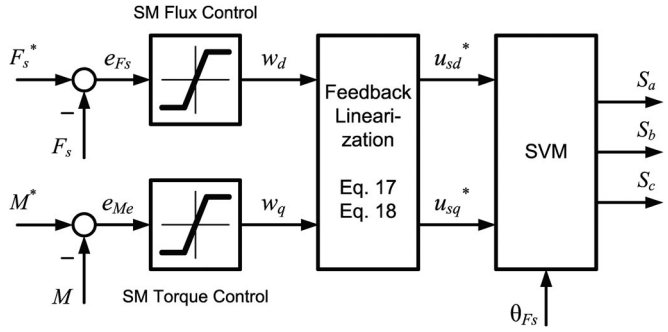

Fig. 2. Torque and flux SMC with feedback linearization for IM control.

IV. Robustness Study and Controller Design

This section provides a design procedure for the sliding-mode FBL controller that achieves robust stability in face of the most important errors, which affect the IM model: motor parameter detuning and speed observation errors. We consider these uncertainties bounded, as in (20) and investigate how these uncertainties impact the choice of corrective gains for torque and flux control. For FBL implementation we use constant motor parameter values and design the controller to remain robust as they change during operation. Rotor speed is obtained from observers with estimation errors, particularly during transients and low speed operation. On the other hand, flux and torque observers give relatively good estimates, and the impact of their errors on FBL is not discussed here.

The errors in the control signal due to these uncertainties are denoted as Δu_{sd} and Δu_{sq}. To evaluate these errors in terms of the rotor speed and parameter errors, and to analyze the effect of uncertainties on the SMC design, we combine (17) and (18) in the following vector form:

$$\underline{u}_s = \left(\frac{w_d}{2R} - \frac{L_m R_s}{L_s L_r - {L_m}^2}\right)\underline{\psi}_r + j\left(\frac{w_q}{R} + \omega_r\right)\underline{\psi}_s. \quad (30)$$

Although w_d and w_q are produced by the SMC and have no uncertainty, we can replace the error in the control signal u_s with equivalent errors in w_d and w_q. The equivalent error is $\Delta w = \Delta w_d + j\Delta w_q$, and (30) can be rewritten as

$$\underline{u}_s = \left(\frac{w_d + \Delta w_d}{2R} - \frac{\hat{L}_m \hat{R}_s}{\left(\hat{L}_m + L_{s\sigma}\right)\left(\hat{L}_m + L_{r\sigma}\right) - \hat{L}_m^2}\right) \underline{\psi}_r + j\left(\frac{w_q + \Delta w_q}{R} + \hat{\omega}_r\right)\underline{\psi}_s \quad (31)$$

where $\hat{L}_m$ is the measured magnetizing inductance, $\hat{R}_s$ is the measured stator resistance, and $\hat{\omega}_r$ is the rotor speed estimate.

Using (30) and (31), the equivalent error is given by

$$\Delta w = \Delta w_d + j\Delta w_q = 2\left(\frac{\hat{L}_m \hat{R}_s}{\left(\hat{L}_m + L_{s\sigma}\right)\left(\hat{L}_m + L_{r\sigma}\right) - \hat{L}_m^2} - \frac{L_m R_s}{L_s L_r - {L_m}^2}\right) R + j\left(\omega_r - \hat{\omega}_r\right) R. \quad (32)$$

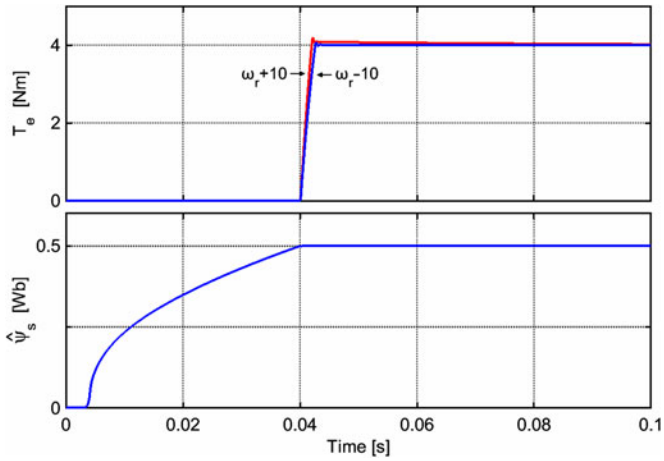

Fig. 3. Simulation results for SMC and FBL with ±10 rad/s speed errors, at startup, torque T_e, and stator flux Ψ_s.

The feedback linearized torque and stator flux dynamics in the presence of errors in w_d and w_q are

$$\frac{dM}{dt} = -\left(\frac{1}{T_r\sigma} + \frac{1}{T_s\sigma}\right)M + w_q - \Delta w_q \quad (33)$$

$$\frac{dF_s}{dt} = -\frac{2}{T_s\sigma}F_s + w_d - \Delta w_d. \quad (34)$$

It can be assumed that the maximum deviation of each uncertain parameter and the maximum measurement or estimation error for the rotor speed are known. For this analysis we use $\eta_M = 10$, $\eta_{F_s} = 10$, which give a realistic dynamic response for torque and flux. The main focus for this section is robust stability rather than dynamic response.

A. Speed (ω_r)

Errors in speed estimation cause model perturbations that may influence the system response. Speed errors have no effect on stator flux dynamics but change the torque (13) to

$$\frac{dM}{dt} = -\frac{1}{\sigma}\left(\frac{1}{T_r} + \frac{1}{T_s}\right)M + \left(\hat{\omega}_r - \omega_r\right)R + w_q. \quad (35)$$

Knowing the maximum speed estimation error, the corrective control gain can guarantee robust performance. The IM has a nominal value of $R, R = 0.25$ (parameters are listed in the Appendix). Assuming a speed measurement with a maximum error of ±10 rad/s (±1.6 Hz), we have $|(\hat{\omega}_r - \omega_r)R| < 2.5$, which corresponds to $G_M = 2.5$ and $k_M = G_M + \eta_M = 12.5$. We use $k_M = 20$, as in our experiments, which handles even larger errors. Since the speed error does not affect the stator flux dynamics, we use $k_{F_s} = \eta_{F_s} + 0 = 10$. Simulation results in Fig. 3 show the torque and flux response for the drive starting from standstill with ±10 rad/s speed errors. The torque control is almost identical for any speed error and it remains stable and ripple-free. For bigger errors, we simply choose a larger gain for robust stability, at the expense of increased chattering.

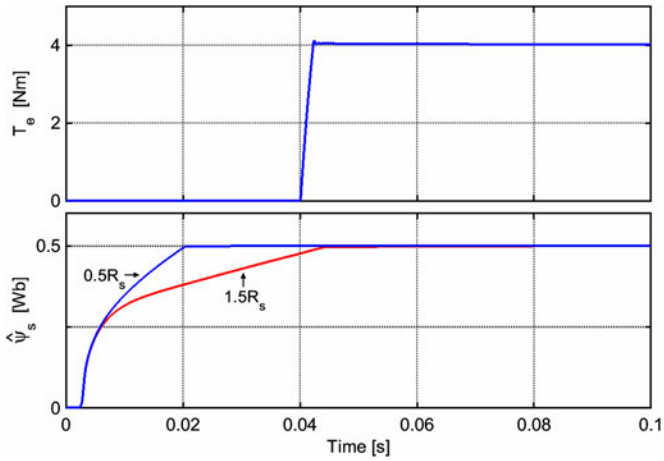

Fig. 4. Simulation results for SMC and FBL with $\pm 50\%$ R_s errors, at startup, torque T_e, and stator flux Ψ_s.

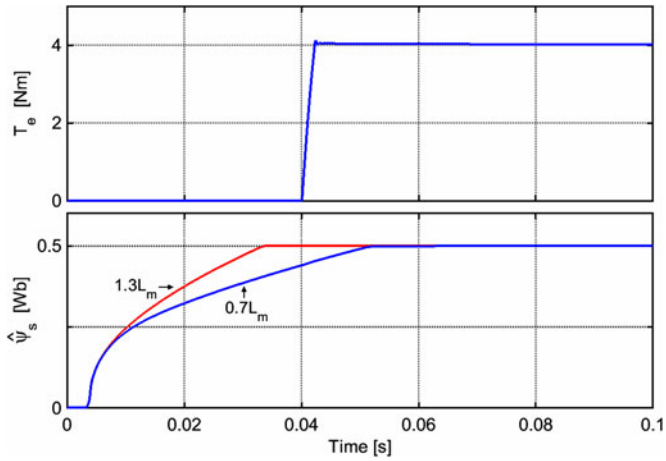

Fig. 5. Simulation results for SMC and FBL with $\pm 30\%$ L_m errors, at startup, torque T_e, and stator flux Ψ_s.

B. Stator Resistance (R_s)

The stator resistance changes with temperature, and it impacts the stator flux dynamics. Introducing a perturbation due to stator resistance error, the stator flux dynamics (34) is given by

$$\frac{dF_s}{dt} = -\frac{2}{T_s\sigma}F_s + \frac{2L_m}{L_r L_s \sigma}R\left(R_s - \hat{R}_s\right) + w_d \qquad (36)$$

where $\hat{R}_s$ is the nominal stator resistance and R_s is its actual value. We consider a maximum error in the stator resistance of $\pm 50\%$, i.e., $|R_s - \hat{R}_s| < 0.5 \times \hat{R}_s = 1.15$. The corresponding model perturbation for the parameter values is $G_{F_s} = \frac{2L_m}{L_r L_s \sigma} R \times 0.69 = 28.16$. We choose the corrective control gain $k_{F_s} = \eta_{F_s} + G_{F_s} = 40 > 38.16$. Since the torque dynamics is independent of the resistance error, we use the same value $k_M = 20$, for similar dynamic performance.

Simulation results in Fig. 4 show the stator flux and torque response for the drive starting from standstill with $\pm 50\%$ stator resistance dynamic uncertainty. Note how the resistance error impacts the flux response time, which is faster for lower resistances and due to larger gain. However, the steady state operation is ripple-free and robust with respect to R_s errors.

C. Rotor Resistance (R_r)

Rotor resistance changes with temperature. The notable advantage of the proposed FBL is that the changes in R_r do not change the dynamics of stator flux and torque and do not affect the control. However, they do change the dynamics of the other two state variables (R, F_r); this substantially impacts the speed estimate. Therefore, the rotor resistance errors are accounted for by speed errors discussed in Section IV-A.

D. Magnetizing Inductance (L_m)

The magnetizing inductance deviates from its measured value due to magnetic saturation. Changes in the magnetizing inductance produce changes in both the stator and rotor inductances. This has no effect on torque dynamics, but changes the stator flux dynamics (34), as follows:

$$\frac{dF_s}{dt} = -\frac{2}{T_s\sigma}F_s + 2RR_s\left(\frac{L_m}{L_s L_r - {L_m}^2} - \frac{\hat{L}_m}{\left(\hat{L}_m + L_{s\sigma}\right)\left(\hat{L}_m + L_{r\sigma}\right) - \hat{L}_m^2}\right) + w_d. \qquad (37)$$

We consider a maximum change in the magnetizing inductance of $\pm 30\%$, i.e., $0.7\,\hat{L}_m \;\; L_m \; 1.3\,\hat{L}_m$. We examine the term

$$\Delta_L = \frac{L_m}{L_s L_r - {L_m}^2} - \frac{\hat{L}_m}{(\hat{L}_m + L_{s\sigma})(\hat{L}_m + L_{r\sigma}) - \hat{L}_m^2}$$

in (37) that depends on L_m. For $L_m = 0.7\,\hat{L}_m$, we have $_L = -0.42467$, and for $L_m = 1.3\,\hat{L}_m$, we have $_L = 0.23176$. For robust stability, we use the maximum value of $|_L|$. The corresponding perturbation is $G_{F_s} = 2RR_s \times 0.42467 = 0.49$. We use the gain $k_{F_s} = 12 > 10.49$. Since the torque dynamics is independent of the magnetizing inductance, we use $k_M = 20$. Simulation results in Fig. 5 show the stator flux and torque for the drive starting from standstill with $\pm 30\%$ magnetizing inductance errors. Again, it is proved that SMC provides robust and ripple-free steady state performance. Overall, the largest gains can be used for all situations. All simulations are for the sensorless drive shown in Fig. 1.

The proposed SMC design is based on the required dynamic response (η_M, η_{F_s}) and the maximum uncertainty (G_M, G_{F_s}). The dynamic response is application dependent and is chosen by the designer. Equation (34) gives the maximum uncertainty caused by FBL. Given η and G for flux and torque, the designer chooses a sliding gain larger than $G_M + \eta_M$ for the torque controller and larger than $G_{F_s} + \eta_{F_s}$ for the flux controller. This choice of the corrective control gains results in a robust and stable system that operates at the required speed while suppressing chattering. Comparing all simulation results, we conclude that larger gains result in a faster and robust control but can cause chattering if the increase in gain is excessive.

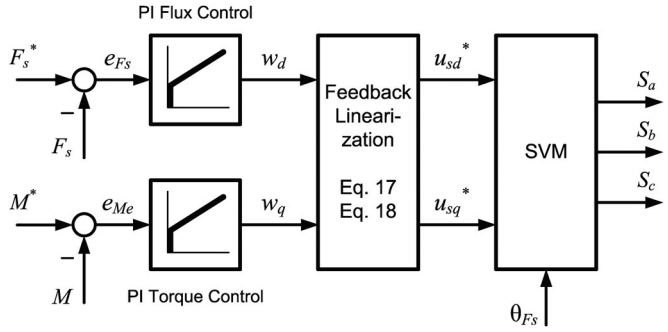

Fig. 6. Torque and flux PI control with feedback linearization for IM control.

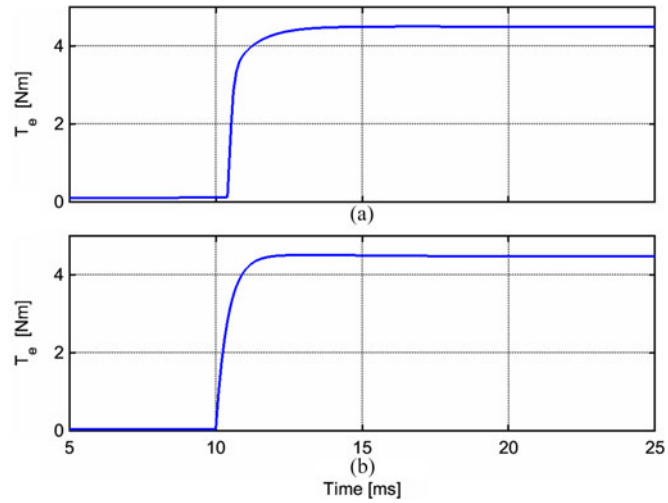

Fig. 7. Torque response to 4.5 N·m step command with (a) PI controllers (linear DTC) and (b) PI controllers and FBL. Startup from standstill.

V. Experimental Results

A. Comparison of Feedback Linearization and Linear DTC

Linear DTC is a control scheme that uses linear proportional–integral (PI) controllers for torque and flux, in order to obtain a good control performance [4]. The new FBL design proposed provides similar or better performance. We first compare the linear PI torque (M) and flux (Fs) control with FBL, whose bloc diagram is shown in Fig. 6, against linear DTC (without FBL).

For a fair comparison, the experiments were performed using the same PI controller gains for both solutions. The torque step response is shown in Fig. 7, and the stator flux step response is shown in Fig. 8. The PI controller with FBL in Fig. 7(b) gives a slightly faster torque response with more accurate steady-state tracking than the linear DTC in Fig. 7(a), at the expense of a small overshoot. Fig. 8(b) shows that the flux response for FBL is slightly faster than the linear DTC in Fig. 8(a). The control performance of the PI with FBL solution shows good dynamic response, but it is not robust. The experimental setup data and controller gains are provided in the Appendix.

B. DTC via Feedback Linearization and Sliding Mode

The proposed sliding-mode controller with FBL has been designed and implemented on the same setup. Its block diagram is shown in Fig. 2. For all tests, we used a very simple flux and torque observer (LPF of the EMF), which produces modest results. Fig. 9. shows the torque response to a 4.5 Nm (1.5 rated torque) step command and the stator flux, during startup from standstill.

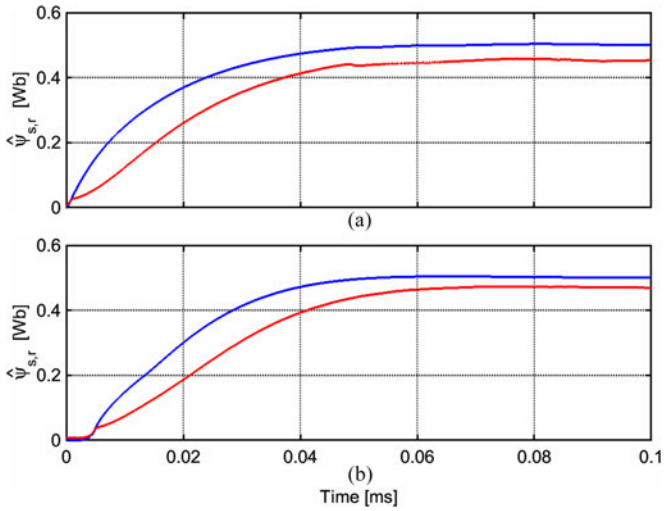

Fig. 8. Stator (blue) and rotor (red) flux magnitude control at startup, with (a) PI controllers (linear DTC) and (b) PI controllers and FBL.

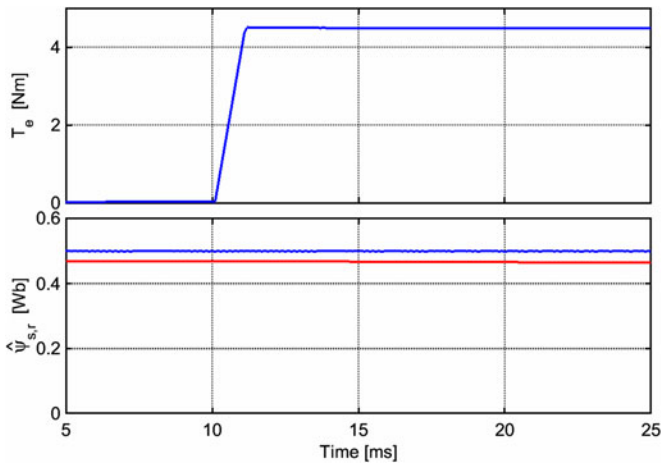

Fig. 9. Torque transients for startup from standstill with feedback linearization and SMC (a) torque and (b) stator and rotor flux magnitudes.

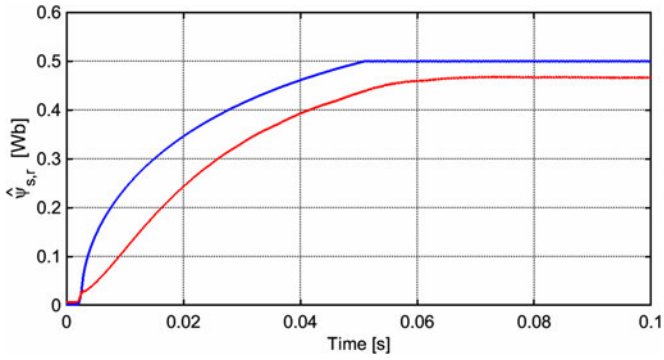

Fig. 10. Stator (blue) and rotor (red) flux magnitude response to 0.5 Wb step command with feedback linearization and SMC, at standstill.

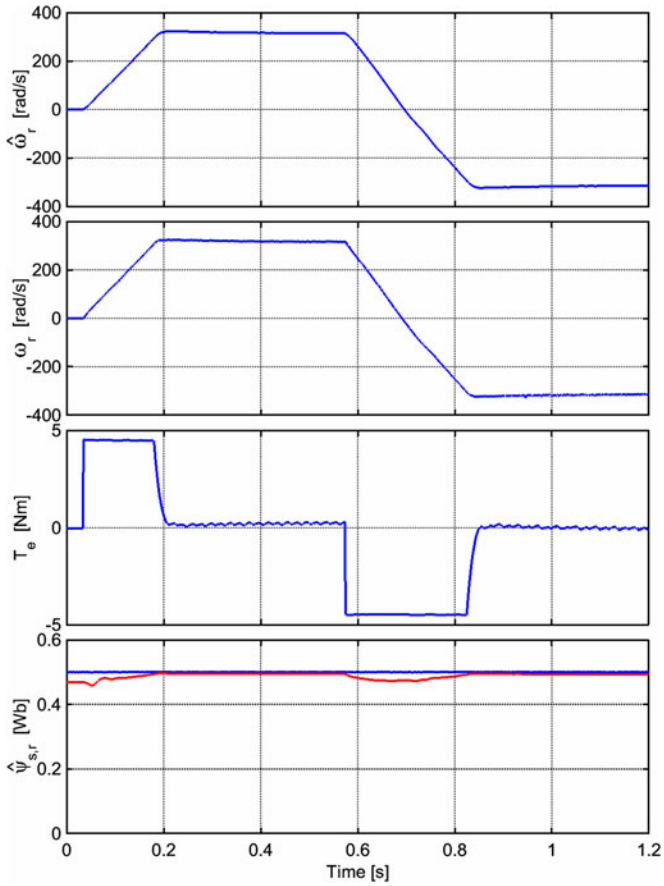

Fig. 11. IM startup and reversal with FBL and SMC (a) estimated speed, (b) measured speed, (c) torque, and (d) stator (blue) and rotor (red) flux magnitudes.

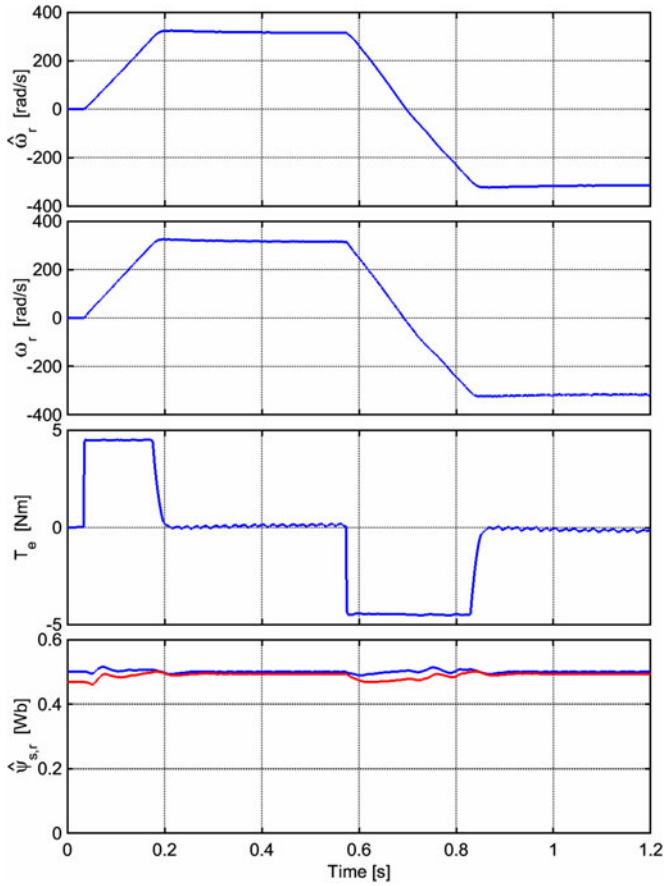

Fig. 12. IM startup with FBL and PI control (a) estimated speed, (b) measured speed, (c) torque, and (d) stator (blue) and rotor (red) flux magnitudes.

The stator flux was preinstalled and its magnitude shows that the FBL effectively decouples the flux and torque. The torque reaches 4.5 Nm in less than 2 ms and the overshoot is negligible with very low steady state ripple. Fig. 10 shows the stator and rotor flux magnitude response to a 0.5 Wb step command for stator flux magnitude. The response is fast and chattering free.

To show the drive behavior under speed control, we use a PI speed controller to generate the torque reference. The acceleration from 0 Hz to 50 Hz followed by a reversal from 50 Hz to -50 Hz are shown in Fig. 11. The figure shows estimated speed, measured speed, torque, and stator and rotor flux magnitudes. Notice how rigidly the flux and torque are kept to their set points during speed transients. For comparison, the same test was run with FBL and PI controllers (see Fig. 6), and the results are shown in Fig. 12.

While the speed response is similar, the torque and stator flux magnitudes in Fig. 12 show oscillations during speed transients, which indicate a lack of robustness and imperfect decoupling for the PI controller. Despite the simple flux and speed observer and other errors, the speed control is fast and accurate in all cases.

Low speed operation with SMC and FBL is illustrated in Fig. 13, which shows fast reversals at ± 3 Hz electrical speed. The torque control is fast, while the stator flux is kept constant, which replicates the same robust behavior as in Fig. 11. For this experiment the flux observer cutoff frequency was decreased to $\omega_0 = 1$ rad/s. Based on the experimental evidence we conclude that the SMC has very robust operation at all speeds.

VI. Conclusion

This paper proposes a new design approach that integrates feedback linearization and SMC with a DTC drive. This new solution based on torque–flux linearization produces an intuitive linear model of the IM, with torque and flux as decoupled state variables. For the linear IM model, the controller–observer separation principle holds if estimation errors are small, which allows the controller and observer to be independently designed. It also allows the use of a simple traditional linear design approach and the use of linear state observers.

Sliding-mode direct torque and flux control provides robustness against parameter uncertainties and their changes, as proved by the comparison with a linear controller. The chattering associated with sliding-mode operation is eliminated by the proportional controller used inside the boundary layer. The drive has the same fast and robust response, as a conventional DTC drive and completely eliminates the torque and flux ripple. Overall, the solution combines the advantages of conventional and linear DTC. These advantages are due to the sliding-mode controller and the linearization, which decouples the torque and stator flux magnitude.

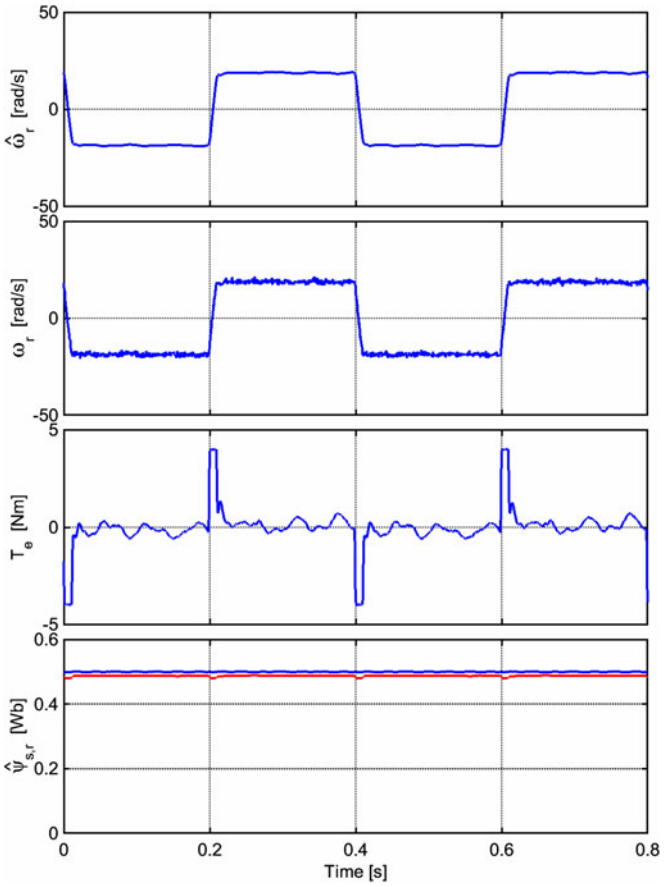

Fig. 13. IM low-speed reversals with FBL and SMC (a) estimated speed, (b) measured speed, (c) torque, and (d) stator (blue) and rotor (red) flux magnitudes.

Extensive experimental results carried out demonstrate that torque–flux feedback linearization is a useful approach to IM drive control. It allows independent design of controllers and observers, and facilitates a relatively simple integration of conventional linear and nonlinear controllers. The use of existing linear observers is also very simple.

APPENDIX
EXPERIMENTAL SETUP

The proposed FBL control has been tested on a 0.75 hp sensorless IM drive, with block diagram shown in Fig. 1. The VSI is a 2.2 kVA FC302 inverter from Danfoss Drives. The control was implemented in *C++* on a TMS320F28335 DSP from Texas Instruments at a sampling and switching frequency of $f_s = 10$ kHz.

The IM nameplate data and parameters are:

$$P_N = 0.75 \text{ hp},\ U_{sN} = 240 \text{ V},\ f_{sN} = 60 \text{ Hz},$$

$$n_N = 1725 \text{ r/min},\ T_{eN} = 3.05 \text{ N} \cdot \text{m},\ p = 2, R_s = 2.3\ \Omega,$$

$$R_r = 2.5\ \Omega,\ L_m = 0.24 \text{ H},\ L_s = L_r = 0.25 \text{ H}.$$

Two currents and the dc-link voltage were measured.

The stator flux is estimated by a simple low pass filter that approximates the EMF integral for frequencies higher than its cutoff frequency: $\underline{\psi}_s = \frac{1}{s+\omega_0}(\underline{u}_s - R_s \underline{i}_s)$, where $\omega_0 = 10\text{rad/s}(f_0 = 1.59\text{Hz})$. This estimator produces modest results, with large errors during speed transients and at low speeds. The rotor speed is estimated as $\hat{\omega}_r = \hat{\omega}_{\psi r} - \hat{\omega}_s$ where $\hat{\omega}_{\psi r}$ is the rotor flux speed calculated as the differential of rotor flux position, and $\hat{\omega}_s = 2R_r T_e/(3p\psi_r^2)$ is the slip speed. We purposely selected a very simple flux and speed observer in order to test the controller performance and its robustness in a realistic practical environment with flux and speed errors.

Control parameters used in the experiments are as follows:

1) PI controllers for linear DTC: $K_{P,F_s} = 50, K_{I,F_s} = 1000, K_{P,T_e} = 15, K_{I,T_e} = 2000$;
2) PI controllers with FBL: $K_{P,F_s} = 50, K_{I,F_s} = 1000, K_{P,T_e} = 6, K_{I,T_e} = 800$;
3) Sliding-mode controllers with FBL: $K_{SMC,F_s} = 5, K_{SMC,T_e} = 20$ with boundary layers $h_{F_s} = 0.01$ Wb, $h_{T_e} = 0.4$ N · m.

REFERENCES

[1] I. Takahashi and T. Noguchi, "A new quick response and high efficiency control strategy of an induction motor," in *Proc. 1985 Annu. Meeting Rec. IEEE IAS*, 1995, pp. 495–502.
[2] G. Buja and M. P. Kazmierkowski, "Direct torque control of PWM inverter-feed AC motors—A survey," *IEEE Trans. Ind. Electron.*, vol. 51, no. 4, pp. 744–757, Aug. 2004.
[3] Y.-S. Lai, W.-K. Wang, and Y.-C. Chen, "Novel switching techniques for reducing the speed ripple of AC drives with direct torque control," *IEEE Trans. Ind. Electron.*, vol. 51, no. 4, pp. 768–775, Aug. 2004.
[4] C. Lascu and A. M. Trzynadlowski, "A sensorless hybrid DTC drive for high-volume low-cost applications," *IEEE Trans. Ind. Electron.*, vol. 51, no. 5, pp. 1048–1055, Oct. 2004.
[5] C. Lascu, I. Boldea, and F. Blaabjerg, "Variable-structure direct torque control—A class of fast and robust controllers for induction machine drives," *IEEE Trans. Ind. Electron.*, vol. 51, no. 4, pp. 785–792, Aug. 2004.
[6] M. P. Kazmierkowski and D. Sobczuk, "High performance induction motor control via feedback linearization," in *Proc. IEEE ISIE*, Jul. 1995, vol. 2, pp. 633–638.
[7] M. P. Kazmierkowski and D. Sobczuk, "Sliding mode feedback linearization of PWM inverter fed induction motor," in *Proc. IEEE IECON*, Aug. 1996, vol. 1, pp. 244–249.
[8] T. K. Boukas and T. G. Habetler, "High-performance induction motor speed control using exact feedback linearization with state and state derivative feedback," *IEEE Trans. Power Electron.*, vol. 19, no. 4, pp. 1022–1028, Jul. 2004.
[9] D. Sobczuk and M. Malinowski, "Feedback linearization control of inverter fed induction motor with sliding mode speed and flux observers," in *Proc. IEEE IECON*, 2006, pp. 1299–1304.
[10] G. Luckjiff, I. Wallace, and D. Divan, "Feedback linearization of current regulated induction motors," in *Proc. IEEE PESC*, 2001, pp. 1173–1178.
[11] J. Chiasson, *Modeling and High-Performance Control of Electric Machines*. New York, NY, USA: Wiley, 2005.
[12] J. Chiasson, "A new approach to dynamic feedback linearization control of an induction motor," *IEEE Trans. Automat. Control*, vol. 43, no. 3, pp. 391–397, Mar. 1998.
[13] Y. S. Choi, H. H. Choi, and J. W. Jung, "Feedback linearization direct torque control with reduced torque and flux ripples for IPMSM drives," *IEEE Trans. Power Electron.*, vol. 31, no. 5, pp. 3728–3737, May 2016.
[14] K. H. Kim, Y. C. Jeung, D. C. Lee, and H. G. Kim, "LVRT scheme of PMSG wind power system based on feedback linearization," *IEEE Trans. Power Electron.*, vol. 27, no. 5, pp. 2376–2384, May 2012.
[15] X. Bao, F. Zhuo, Y. Tian, and P. Tan, "Simplified feedback linearization control of three-phase photovoltaic inverter with an LCL filter," *IEEE Trans. Power Electron.*, vol. 23, no. 3, pp. 2739–2752, Jun. 2013.
[16] P. Liutanakul, S. Pierfederici, and F. M. Tabar, "Application of SMC with I/O feedback linearization to the control of the cascade controlled-rectifier/inverter-motor drive system with small DC link capacitor," *IEEE Trans. Power Electron.*, vol. 23, no. 5, pp. 2489–2499, Oct. 2008.

[17] H. A. Zarchi, J. Soltani, and G. A. Markadeh, "Adaptive input–output feedback-linearization-based torque control of synchronous reluctance motor without mechanical sensor," *IEEE Trans. Ind. Electron.*, vol. 57, no. 1, pp. 375–384, Jan. 2010.
[18] D. E. Kim and D. C. Lee, "Feedback linearization control of three-phase UPS inverter systems," *IEEE Trans. Ind. Electron.*, vol. 57, no. 3, pp. 963–968, Mar. 2010.
[19] J. Matas, M. Castilla, J. M. Guerrero, L. G. de Vicuna, and J. Miret, "Feedback linearization of direct drive synchronous wind turbines via a sliding mode approach," *IEEE Trans. Power Electron.*, vol. 23, no. 3, pp. 1093–1103, May 2008.
[20] J. Matas, L. G. de Vicuna, J. Miret, J. M. Guerrero, and M. Castilla, "Feedback linearization of a single-phase active power filter via sliding mode control," *IEEE Trans. Power Electron.*, vol. 23, no. 1, pp. 116–125, Jan. 2008.
[21] V. Utkin, J. Guldner, and J. Shi, *Sliding Mode Control in Electromechanical Systems*. New York, NY, USA: Taylor & Francis, 1999.
[22] Z. Yan, C. Jin, and V. I. Utkin, "Sensorless sliding-mode control of induction motors," *IEEE Trans. Ind. Electron.*, vol. 47, no. 6, pp. 1286–1297, Dec. 2000.
[23] K. Jezernik, J. Korelic, and R. Horvat, "PMSM sliding mode FPGA based control for torque ripple reduction," *IEEE Trans. Power Electron.*, vol. 28, no. 7, pp. 3549–3556, Jul. 2013.
[24] R. Ling, D. Maksimovic, and R. Leyva, "Second order sliding mode controlled synchronous buck DC–DC converter," *IEEE Trans. Power Electron.*, vol. 31, no. 3, pp. 2539–2549, Mar. 2016.
[25] L. Del Re and A. Isidori, "Performance enhancement of nonlinear drives by feedback linearization of linear-bilinear cascade models," *IEEE Trans. Control Syst. Technol.*, vol. 3, no. 3, pp. 299–308, Sep. 1995.
[26] M. Fatu, C. Lascu, G.-D. Andreescu, R. Teodorescu, F. Blaabjerg, and I. Boldea, "Voltage sags ride-trough of motion sensorless controlled PMSG for wind turbines," *in Proc. 42nd IEEE IAS Annu. Meeting*, 2007, vol. 1, pp. 171–178.
[27] M. Sami Fadali, "Continuous drug delivery system design using nonlinear decoupling: A tutorial," *IEEE Trans. Biomed. Eng*., vol. BME-34, no. 9, pp. 650–653, Aug. 1987.

Cristian Lascu received the B. S., M.Sc., and Ph.D. degrees in electrical engineering from the University Politehnica of Timisoara, Timisoara, Romania, in 1994, 1995, and 2002, respectively.

Since 1995, he has been with the Department of Electrical Engineering, University Politehnica of Timisoara. He was a Visiting Researcher with the Institute of Energy Technology, Aalborg University, Aalborg, Denmark on several occasions. From 2002 to 2004, he was with SIEI S.p.A., Italy, where he was engaged in advanced power electronics and drives for electrical vehicles under a European Marie Curie Fellowship. From 2009 to 2011, he was with the Department of Electrical and Biomedical Engineering, University of Nevada Reno, Reno, NV, USA. His current research interests include power electronics and high-performance electrical drives.

Dr. Lascu was a recipient of an IEEE Industry Applications Society Prize Paper Award in 1998.

Saeed Jafarzadeh (M'09) received the Ph.D. degree from the University of Nevada Reno, Reno, NV, USA, in 2012.

Since 2012 he has been an Assistant Professor with the Department of Computer and Electrical Engineering and Computer Science, California State University Bakersfield, Bakersfield, CA, USA. His current research interests include fuzzy systems, stability analysis, nonlinear control and their application to power systems, induction motor control, and renewable energy systems.

M. Sami Fadali (SM'91) received the B.S. degree in electrical engineering from Cairo University, Cairo, Egypt, the M.Sc. degree from the Control Systems Center, University of Manchester Institute of Science and Technology, Manchester, U.K., and the Ph.D. degree from the University of Wyoming, Laramie, WY, USA.

He was an Assistant Professor of Electrical Engineering with the University of King Abdul Aziz, Jeddah, Saudi Arabia, then a Postdoctoral Fellow at Colorado State University, Fort Collins, before joining the University of Nevada Reno, Reno, NV, USA, where he is currently a Professor and Chair of the Electrical and Biomedical Engineering Department. His current research interests include in the areas of fuzzy logic stability and control, state estimation, and fault detection.

Dr. Fadali is an Associate Editor of the IEEE TRANSACTIONS ON FUZZY SYSTEMS.

Frede Blaabjerg (S'86–M'88–SM'97–F'03) received the Ph.D. degree from Aalborg University, Aalborg, Denmark, in 1992.

He was with ABB-Scandia, Randers, Denmark, from 1987 to 1988. He became an Assistant Professor in 1992, Associate Professor in 1996, and Full Professor of power electronics and drives in 1998. He is currently with Aalborg University, Aalborg East, Denmark. His current research interests include power electronics and its applications such as in wind turbines, PV systems, reliability, harmonics and adjustable speed drives.

Dr. Blaabjerg has received 17 IEEE Prize Paper Awards, the IEEE PELS Distinguished Service Award in 2009, the EPE-PEMC Council Award in 2010, the IEEE William E. Newell Power Electronics Award 2014, and the Villum Kann Rasmussen Research Award 2014. He was an Editor-in-Chief of the IEEE TRANSACTIONS ON POWER ELECTRONICS from 2006 to 2012. He was nominated in 2014 and 2015 by Thomson Reuters to be between the most 250 cited researchers in engineering in the world.